

**RESONANT FARADAY ROTATION
IN A HOT LITHIUM VAPOR**

By

SCOTT RUSSELL WAITUKAITIS

A Thesis Submitted to The Honors College

In Partial Fulfillment of the Bachelors degree
With Honors in

Physics

THE UNIVERSITY OF ARIZONA

MAY 2007

Approved by:

Dr. Alex Cronin
Department of Physics

STATEMENT BY AUTHOR

This thesis has been submitted in partial fulfillment of requirements for a degree at The University of Arizona and is deposited in the University Library to be made available to borrowers under rules of the Library.

Signed:-----

Abstract

I describe a study of Faraday rotation in a hot lithium vapor. I begin by discussing the experimental setup used to infer Faraday rotation. Next, I present a theoretical framework to understand why the rotation occurs. Measured data is compared to the theoretical model, and it is seen that the two have only qualitative agreement. I conclude by addressing issues which could be probed to improve agreement between the model and the data in further work.

Contents

1	Introduction	3
2	Experimental Hardware and Setup	5
2.1	General Setup and Procedure	5
2.2	The Laser	5
2.3	The Lithium Oven and Solenoid	7
3	Theoretical Framework for Faraday Rotation in a Hot Lithium Vapor	8
3.1	Superposition of σ_+ and σ_- Light	8
3.2	Line Shapes for $\alpha(\nu)$ and $n(\nu)$	9
3.3	The Role of the Zeeman Effect	10
3.4	Faraday Rotation in Lithium	11
3.4.1	Relation Between Theory and Observed Quantities	11
3.4.2	Broadening Mechanisms	13
3.4.3	Energy Levels in Lithium	14
4	Observed Faraday Rotation Spectra	16
4.1	Analysis of Observed Faraday Rotation Spectra	16
5	Computer Model for Observed Data	19
5.1	Construction of the Model	19
5.2	Comparison of the Model with Data	20
5.3	Possible Improvements on Model and Data	20
6	Conclusion and Outlook	22

List of Figures

1.1	Conceptual diagram of Faraday rotation	4
2.1	Experimental setup	6
3.1	Index and absorption vs. ν	10
3.2	Zeeman splitting in a four level system	11
3.3	Faraday rotation in a simple system	12
3.4	Atomic energy levels of lithium	15
4.1	Faraday rotation spectra and model	18

Chapter 1

Introduction

Faraday rotation is the change in the plane of polarization of light passing through a medium in which there is an applied magnetic field in the direction of light propagation. This is illustrated in Fig. 1.1. Michael Faraday discovered this magneto-optical rotation in a series of experiments carried out in 1845. Faraday sent polarized light through a glass slab and noticed that the plane of polarization rotated when a magnetic field was applied [12]. Mathematically, Faraday found that rotation in glass is proportional to both the magnetic field strength B and to the length of the glass slab D , i.e.

$$\Delta\theta = VBD \tag{1.1}$$

where V is known as the Verdet constant with units $^\circ\text{Gauss}^{-1}\text{m}^{-1}$ [8].

In the last 150 years, much more has been discovered regarding Faraday rotation. It is now known that Faraday rotation is related to the Zeeman effect. It is also known that the so-called Verdet constant is frequency-dependent and can be especially large near atomic resonances. For this reason, Faraday rotation in atomic vapors has become a subject of practical theoretical and experimental interest. One benefit of working with atomic vapors is that they are well understood theoretically. Furthermore, physical parameters that would be difficult to manipulate in a solid, such as number density, are easily manipulated in a vapor.

Faraday rotation has also found practical uses in the laboratory and industry. For example, Faraday rotation is implemented in magnetometers [5] and narrow-bandpass optical transmission filters [9, 10].

This thesis describes Faraday rotation spectra obtained with a dilute lithium vapor and a diode laser tuned near the D_1 and D_2 resonance lines.

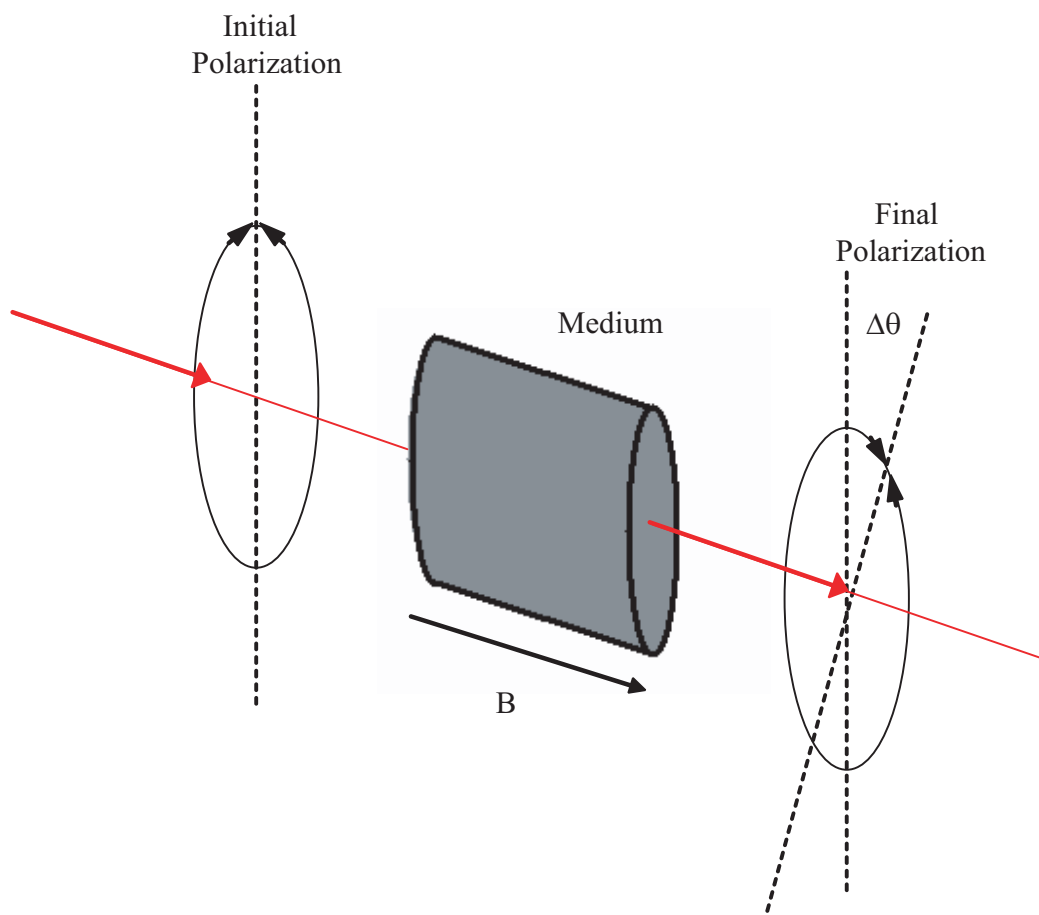


Figure 1.1: After interacting with the medium under the influence of the magnetic field, the plane of polarization changes by amount $\Delta\theta$.

The topics covered are of (1) the experimental hardware and setup, (2) the theoretical framework for the Faraday rotation in an atomic vapor, (3) analysis and discussion of observed Faraday rotation, (4) comparison of observed spectra to theoretically predicted spectra, and (5) conclusion and an outlook toward future investigations.

Chapter 2

Experimental Hardware and Setup

2.1 General Setup and Procedure

The experimental setup is presented in Fig. 2.1. The main components are a tunable 670 nm diode laser, a polarizer, a heat pipe oven, a solenoid surrounding the oven, a polarizing beam splitter cube (PBS), two photodetectors and a computer.

The Faraday rotation spectra are obtained in the following way. First, the laser frequency is modulated to scan a ~ 40 GHz range centered on the D_1 line of ${}^7\text{Li}$. This is accomplished with a function generator ramping both the laser current and the external cavity length. The laser light passes through a polarizer set 45° relative to both axes of the PBS. The light passes through the oven and interacts with the lithium atoms. When it reaches the PBS, the horizontal component is sent to photodetector #1 and the vertical component to photodetector #2. The difference of these signals is taken via a homemade difference amplifier. This signal is indicative of Faraday rotation and is recorded by the computer.

2.2 The Laser

The laser used was the Sanyo DL3149-057 which has a typical maximum output of 7 mW and a typical lasing wavelength of 670 nm. Measured values of the output power at a current of 35 mA were slightly lower at ~ 4 mW.

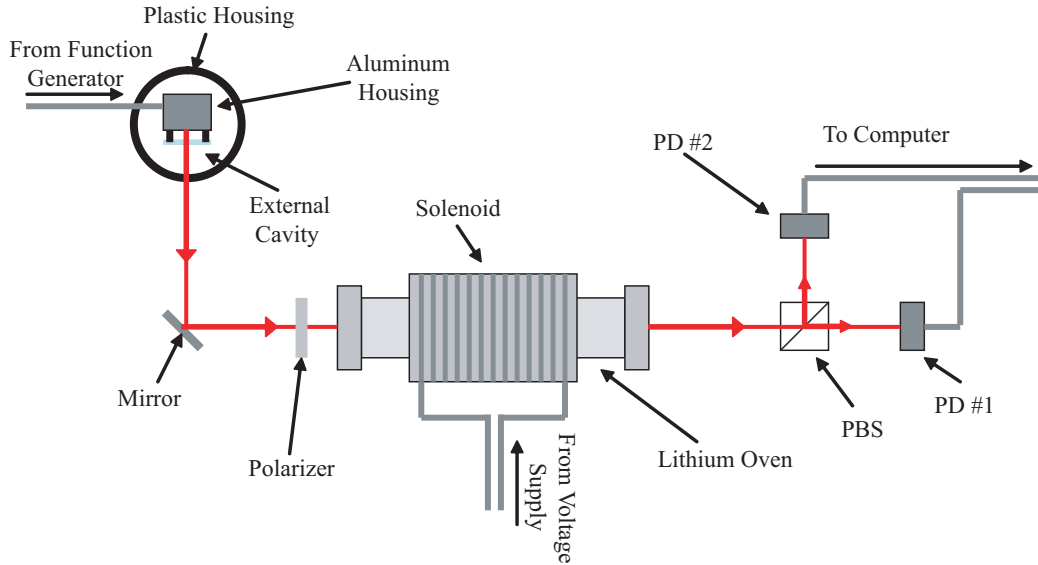


Figure 2.1: The laser beam is polarized at 45° relative to axes of the PBS when the magnetic field is off. When the magnetic field is on, the Faraday rotation causes the signal at one photodetector to be larger than the signal at the other. The difference of these signals is recorded by the computer.

The laser housing consisted of a block of aluminum which was temperature stabilized with a feedback circuit. For additional temperature stabilization, this unit was kept inside a plastic container which protected it from circulating air. The laser current was regulated with a protection circuit which prevented impulsive currents or reverse currents from destroying the unit. The laser was ramped in triangle mode with a function generator.

The DL3149-057 has a mode-hop free range of $\sim 5 - 10$ GHz. For the lithium D_1 and D_2 transitions a range of ~ 30 GHz was required. To achieve this range a piezo-electric external cavity was placed in front of the laser. This cavity was built out of a microscope slide and two ThorLabs AE0203D04F piezo electric actuators. The cavity suppressed mode hops by modulating its length with the same frequency and nearly the same phase as the laser current modulation. Using this technique the mode-hop free range was increased to ~ 40 GHz.

For a more detailed discussion of the laser system, the reader is directed to [4, 13].

2.3 The Lithium Oven and Solenoid

The lithium oven used was a cylindrical steel pipe which measured 38.5 cm long by 1.5 cm in radius. Glass windows on the ends of the pipe allowed the laser to enter and exit from both sides. An argon buffer gas was used to keep the lithium concentrated in the center of the oven.

The oven was evacuated to a room temperature pressure of 10^{-5} torr. The oven was heated with a resistive wire heater. Typical operating temperatures were around $350^{\circ} - 425^{\circ}\text{C}$.

The solenoid used was made from a hollow aluminum cylinder ~ 10 cm in diameter and 10 cm long. Magnet wire was wound around this tube 100 times forward and 100 times backward in the same sense. This made for a solenoid of 20 turns/cm. This arrangement was capable of producing a magnetic field strength of 20 – 50 Gauss near its center with a ~ 5 A current.

Chapter 3

Theoretical Framework for Faraday Rotation in a Hot Lithium Vapor

3.1 Superposition of σ_+ and σ_- Light

Faraday rotation can be related to a difference in the index of refraction for the σ_+ and σ_- polarizations, which describe right-hand circularly polarized and left-hand circularly polarized light, respectively. This section will show how a difference in these indices can lead to an overall polarization rotation.

The laser light is approximated as a monochromatic linearly polarized beam. If the plane of polarization is chosen to be the xy-plane and the axis of propagation is chosen to be the z-axis, then this beam is described in the σ_+ and σ_- basis by

$$\vec{E}(z, t) = \frac{E_0}{2}(\hat{x} + i\hat{y})e^{\frac{-z\alpha_+(\nu)}{2}}e^{i2\pi(\frac{zn_+(\nu)}{\lambda_0} - \nu t)} + \frac{E_0}{2}(\hat{x} - i\hat{y})e^{\frac{-z\alpha_-(\nu)}{2}}e^{i2\pi(\frac{zn_-(\nu)}{\lambda_0} - \nu t)} \quad (3.1)$$

where consideration of the real part only is implied. The first term on the right hand side of Eq. (3.1) describes the σ_+ beam, and the second describes the σ_- beam. At $z = 0$ the light is linearly polarized along \hat{x} . If the absorptivities of each polarization are nearly equal, then the emergent beam is linearly polarized, but its plane of polarization is rotated. Take the length of the medium to be D . The emergent light is described by

$$\vec{E}(D, t) = E_0 e^{\frac{-\alpha(\nu)D}{2}} [\hat{x} \cos(\Delta\theta) - \hat{y} \sin(\Delta\theta)] e^{i\left(\frac{2\pi D}{\lambda_0} \left(\frac{n_+ + n_-}{2}\right) - 2\pi\nu t\right)}. \quad (3.2)$$

The angle $\Delta\theta$ is the Faraday rotation angle, and is given by

$$\Delta\theta = \frac{\pi D}{\lambda_0} (n_+(\nu) - n_-(\nu)). \quad (3.3)$$

As claimed, the cause of Faraday rotation can be traced to a difference between $n_+(\nu)$ and $n_-(\nu)$ [14].

3.2 Line Shapes for $\alpha(\nu)$ and $n(\nu)$

The indices of refraction $n_+(\nu)$ and $n_-(\nu)$ in Eq. (3.1) are assumed to depend on ν . If they were constants, the rotation would also be constant; this would be dull thesis indeed. In a dilute atomic vapor at frequencies near atomic resonances, however, these indices have very sensitive to ν . To make things more interesting, the absorptivity $\alpha(\nu)$ also depends on the frequency. This section will explain the shapes of these functions.

If most of the atoms are in the ground state, then the absorption coefficient as a function of ν is proportional to the number density of particles in the ground state, the integrated cross section for absorption, and the Lorentzian line-shape function $g(\nu)$:

$$\alpha(\nu) = n_g \sigma_0 g(\nu) = n_g \sigma_0 \frac{(\gamma_0/4\pi)^2}{(\nu_0 - \nu)^2 + (\gamma_0/4\pi)^2} \quad (3.4)$$

The term $\gamma_0/2\pi$ is the natural linewidth of the transition (MHz) and ν_0 is the resonant frequency of the transition (GHz).

The refractive index as a function of ν is a dispersion profile centered on the atomic resonance [2]

$$n(\nu) - 1 = n_g \sigma_0 \frac{\lambda \gamma_0}{8\pi^2} \frac{(\nu_0 - \nu)}{(\nu_0 - \nu)^2 + (\gamma_0/4\pi)^2}. \quad (3.5)$$

Graphs of the absorption and index for a single transition are presented in Fig. 3.1. As Eq. (3.3) indicates the shapes of the index of refraction profiles are directly related to the shape of the Faraday rotation spectra. With an intricate arrangement of atomic energy levels, such as the D_1 and D_2 lines of lithium, many transitions are possible. This leads to Faraday rotation spectra which are very interesting and complex (see Fig. 4.1).

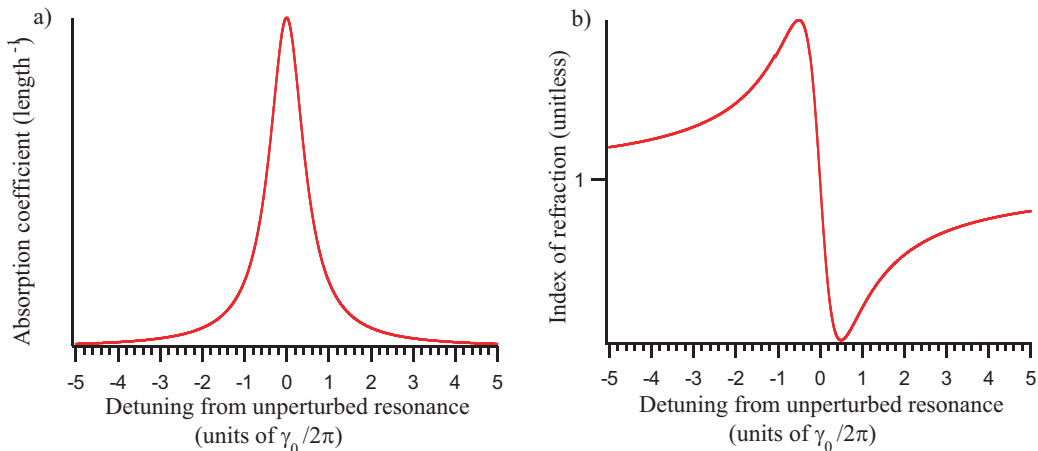


Figure 3.1: Graphs of (a) the refractive index and (b) the absorption as a functions of detuning from a resonance. The x-axis for each graph is in units of natural linewidth ($\gamma_0/2\pi$). They y-axes are intentionally left unscaled.

3.3 The Role of the Zeeman Effect

Conservation of angular momentum dictates which interactions are possible between the light and the atoms. Photons with σ_+ polarization carry angular momentum $+\hbar$ and cause transitions from fine structure angular momentum states $m_J \rightarrow m_J+1$. Photons of σ_- light cause transitions from $m_J \rightarrow m_J-1$. If no magnetic field is present, the m_J energy eigenstates of the atoms are degenerate, and thus the resonant frequencies and indices of refraction for the σ_+ and σ_- polarizations are identical. In the presence of a magnetic field, the degeneracy in m_J is lifted. In this research the strength of the applied magnetic field is small (~ 30 Gauss) in comparison to magnetic field associated with the fine structure correction (~ 3000 Gauss). In this regime, the energy splittings are predicted by the weak field Zeeman effect

$$\Delta E = g_J \mu_B m_J B, \quad (3.6)$$

where g_J is the Landé g-factor (unitless), μ_B is the Bohr magneton (eV/Gauss), and B is the magnetic field strength (Gauss). For a simple four-level system, it is easy to see how the Zeeman effect changes the index of refraction for the σ_+ and σ_- light. Fig. 3.2 shows the energy levels such a system at zero and non-zero magnetic field strengths. As the figure shows, the m_J selection rule



Figure 3.2: Before application of the magnetic field, $\nu_{0,+} = \nu_{0,-}$. After the magnetic field is turned on, $\nu_{0,+} \neq \nu_{0,-}$. This shifts the σ_+ resonant frequencies to higher values and the σ_- resonant frequencies to lower values.

coupled with the m_J dependent Zeeman shifts cause the resonant frequencies for the two polarizations to differ. If we use two different profiles for $n_+(\nu)$ and $n_-(\nu)$ as given by Eq. (3.5) with close, but different, resonant frequencies $\nu_{+,0}$ and $\nu_{-,0}$ in the predicted Faraday rotation (Eq. (3.3)), the result is the shape of the rotation near the unperturbed resonance. This is illustrated in Fig. 3.3.

3.4 Faraday Rotation in Lithium

The transition to a hot, multilevel system comes with the inclusion of a few added complexities. First, broadening mechanisms increase the width and change the shape of the absorption and index of refraction profiles. Second, the real atoms have complex energy level structure which gives rise to many possible transitions.

3.4.1 Relation Between Theory and Observed Quantities

In taking measurements to infer Faraday rotation, it is the time averaged power of the transmitted light that is measured, not the instantaneous value of the electric field (as in Eq. (3.1)). If $\alpha(\nu)$ is assumed to be constant over the length of the medium, then the power of the beam as a function distance

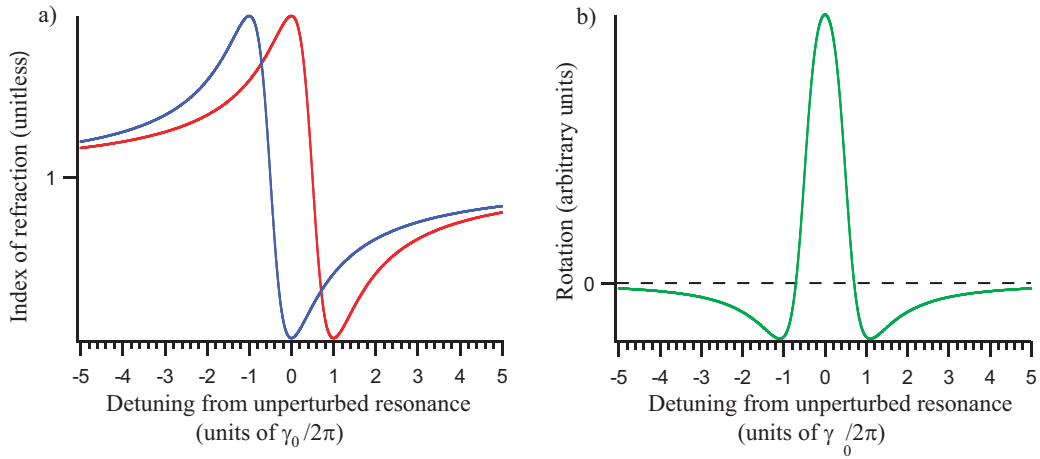


Figure 3.3: Graphs of (a) the index of refraction for σ_+ (red) and σ_- (blue) light and (b) the Faraday rotation signal (green). The y-axes are left unscaled intentionally. The x-axes are given in units of $\gamma_0/2\pi$.

traveled is expressed in the Beer-Lambert law

$$P_t(z, \nu) = P_0(\nu)e^{-\alpha(\nu)D}. \quad (3.7)$$

If a PBS is used downstream from the vapor (as in Fig. 2.1), then the intensities of the horizontal and vertical components of the light can be measured independently. With a polarizer placed upstream at 45° relative to the PBS axes, the difference of the horizontal and vertical intensities should be zero unless rotation has occurred. In this way the difference signal can be used as a proxy to detect Faraday rotation.

3.4.2 Broadening Mechanisms

Several mechanisms account for the far broader spectra observed in experiment than predicted by the theory thus laid out. These mechanisms include Doppler broadening, power broadening, pressure broadening, transit time broadening and laser linewidth broadening.

Doppler broadening is the most dominant source of broadening. This effect occurs because the atoms are moving relative to the lab frame. The atoms in consideration are at a temperature of $\sim 400^\circ \text{C}$, which implies typical speeds of $\sim 1500 \text{ m/s}$. Atoms moving against the direction of light propagation will be resonant with bluer light in the lab frame than atoms moving with the direction of light propagation. This can be accounted for by convolving the cold index of refraction profile (Eq. (3.5)) with the Maxwell-Boltzman velocity distribution of the gas. The velocity of each particle is (to a first approximation) related linearly with the velocity-dependent resonant frequency by

$$\nu_0(v) = \nu_0 \left(1 + \frac{v}{c} \right), \quad (3.8)$$

where ν_0 is the resonant frequency for a stationary atom and v the velocity. The velocity is taken to be positive if the atom is moving against the direction of light propagation and negative if it is moving with the light. Solving for the velocity as a function of ν and rewriting the velocity distribution as a frequency distribution results in a frequency dependent distribution

$$P(\nu)d\nu = \frac{c}{\nu_0 v_p \sqrt{\pi}} e^{\left(\frac{c(\nu - \nu_0)}{\nu_0 v_p} \right)^2} d\nu. \quad (3.9)$$

The parameter $v_p = \sqrt{2k_B T/M}$ is the most probable velocity. The halfwidth of this profile is

$$\Delta\nu_D = \frac{2\nu_0 v_p \sqrt{\ln 2}}{c}. \quad (3.10)$$

For lithium at 400°C this width is $\sim 3000 \text{ MHz}$, making it ~ 500 times larger than the natural linewidth of the lithium transitions ($\sim 6 \text{ MHz}$) [7] [11].

Power broadening occurs when the number of atoms in the excited state becomes comparable to the number of atoms in the ground state. The result of this population distribution is to increase the linewidth of the atomic transition while maintaining the Lorentzian profile. The increase in the linewidth

is given by

$$\gamma = \gamma_0 \sqrt{1 + I/I_s}, \quad (3.11)$$

where I is the intensity of the laser, I_s is the saturation intensity of the atoms, and γ_0 is the natural linewidth in rad s^{-1} [11].

The population in the excited states can also be increased by collisional excitations. This also leads to an increased linewidth, which can be approximated by the linear relationship

$$\gamma = \gamma_0 + aP. \quad (3.12)$$

Here a is a function the collisional cross section of the atoms, the temperature, and the mass [7].

Other broadening mechanisms include transit time broadening and laser linewidth broadening. Transit time broadening stems from the uncertainty principle and the finite interaction time of moving atom with the laser beam [3]. Laser linewidth broadening arises from the fact that the laser is not monochromatic and therefore excites a range of velocity classes at any instant.

3.4.3 Energy Levels in Lithium

The transitions probed by the laser in this experiment are the D_1 and D_2 lines in ${}^6\text{Li}$ and ${}^7\text{Li}$. The energy level diagram for these transitions is shown in Fig. 3.4. For this research, only the fine structure is considered. Considering the structure at this depth involves 8 energy levels for each isotope (4 for the $2^2\text{P}_{3/2}$ manifold and 2 for both the $2^2\text{P}_{1/2}$ and $2^2\text{S}_{1/2}$ manifolds). The m_J selection rule gives rise to a total of 12 allowed transitions: 2 associated with the D_1 line and 4 associated with the D_2 line of each isotope.

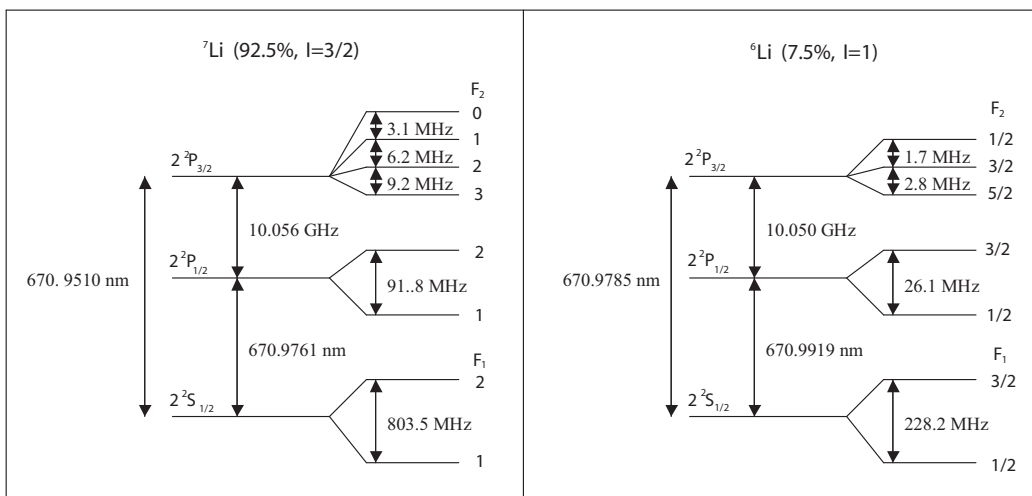


Figure 3.4: The energy levels, nuclear spins and natural abundances of ${}^7\text{Li}$ and ${}^6\text{Li}$ are presented. The figure is not to scale.

Chapter 4

Observed Faraday Rotation Spectra

4.1 Analysis of Observed Faraday Rotation Spectra

Data for the Faraday rotation was taken at several different temperatures ranging from 350 – 425°C and a magnetic field strength of ~ 30 Gauss. The temperature was varied to investigate the effect of different optical depths and different Doppler widths on the spectra. Figure 4.1 shows the total transmitted intensity $I_1 + I_2$ and the difference signal $I_1 - I_2$ for four different temperatures. The frequency-dependent rotation is revealed in the nonzero, frequency-dependent difference signal.

At lower temperatures there is a noticeable positive difference at ~ 0 GHz and ~ 10 GHz which is not present at higher temperatures. This can be understood by taking into account the corresponding absorption profiles for the higher temperature data. As can be seen, the absorption features at ~ 0 GHz and ~ 10 GHz in the $T = 397^\circ\text{C}$ and $T = 420^\circ\text{C}$ data are “bottomed-out”. The fact that this occurs at ~ 0.107 mW implies this amount of the laser light is off-resonant and does not interact with the atoms. When both the on-resonant σ_+ and σ_- beams are “bottomed-out”, their difference is zero and so is the signal. In reality a large Faraday rotation should be occurring at these frequencies, but since all of the light is absorbed the difference $I_1 - I_2$ is small and the rotation is difficult to infer.

Another prominent trend is the increase in rotation in the line wings at

higher temperatures. This can be explained in terms of two mechanisms [6]. First, the rotation is higher because the rotation is proportional to the number density, and as the temperature rises more lithium is present. Second, far away from the resonance (i.e. in the line wings) we have $n(\nu) \propto 1/\nu$ and $a(\nu) \propto 1/\nu^2$. Note in Fig. 4.1 the features near ~ 5 GHz and ~ -5 GHz are not “bottomed-out” by a strong absorption *and* have a large difference $I_1 - I_2$.

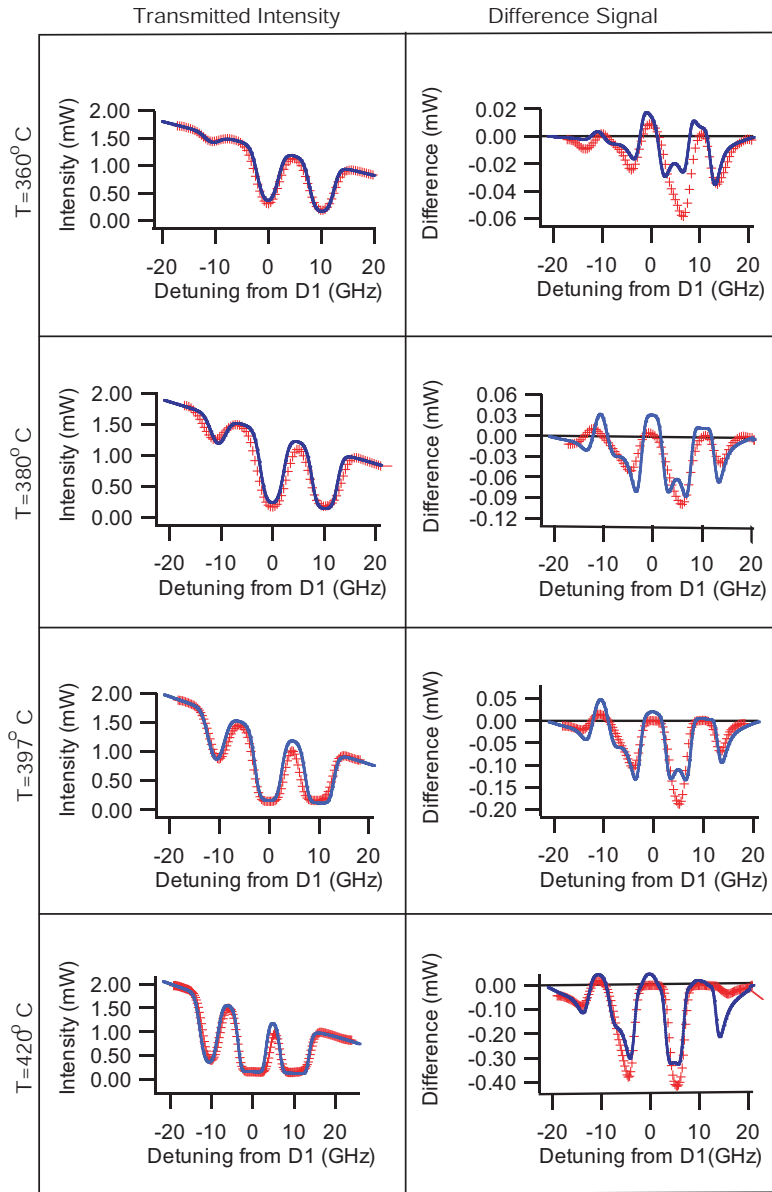


Figure 4.1: Graphs of total transmitted intensity and difference signal at $T = 360^\circ\text{C}$, $T = 380^\circ\text{C}$, $T = 397^\circ\text{C}$, and $T = 420^\circ\text{C}$. The data is shown as red markers and the theory is shown as blue lines. The magnetic field strength was ~ 30 Gauss. The x-axes are given in detuning from ${}^7\text{Li } D_1$. The y-axes for the transmitted intensity and difference signal are in mW.

Chapter 5

Computer Model for Observed Data

5.1 Construction of the Model

The theoretical predictions in Fig. 4.1 were generated with an Igor computer model. This section explains how this computer model was made.

First, a zero temperature optical depth profile $\delta(\nu) = \alpha(\nu)D$ for σ_+ and σ_- light were made by summing over terms similar to Eq. (3.4) for each allowed transition, i.e.

$$\delta(\nu) = C \sum_{i=1}^N \sigma_{0,i} \frac{(\gamma/4\pi)^2}{(\nu_{0,i} - \nu)^2 + (\gamma/4\pi)^2}, \quad (5.1)$$

where N is the total number of transitions and C is a free parameter used in favor of the product nD . Additionally the linewidth $\gamma/4\pi$ was left as a free parameter to account for pressure and power broadening.

The zero temperature index of refraction profile was made in a similar way. The summation for the index of refraction profile was made with terms similar to Eq. (3.5):

$$n(\nu) - 1 = C \frac{\lambda\gamma}{8\pi^2 D} \sum_{i=1}^N \sigma_{0,i} \frac{\nu_{0,i} - \nu}{(\nu_{0,i} - \nu)^2 + (\gamma/4\pi)^2}. \quad (5.2)$$

The C in this equation is the same as in Eq. (5.1). The extra factor $\lambda/2\pi D$ accounts for the ratio between the maximum value of the index of refraction

to the maximum value of the optical depth. Since the region over which the lithium was concentrated was not known, D was left as a free parameter.

The values for $\nu_{0,i}$ were found by adding the energy change due to the weak field Zeeman splitting to the previously determined energy spacings, i.e.

$$\nu_{0,i} = (E_{0,i} + g_{J,e}\mu_B m_{J,e}B + g_{J,g}\mu_B m_{J,g}B)/h. \quad (5.3)$$

The h is Planck's constant. The subscripts e and g indicate the excited and ground states. The Landé-g factors were calculated for each state according to [7]

$$g_J \approx 1 + \frac{J(J+1) - L(L+1) + S(S+1)}{2J(J+1)}. \quad (5.4)$$

Doppler broadening was accounted for by convolving the optical depth and index of refraction profiles with a normalized frequency distribution as given in Eq. (3.9). The value for ν_0 in the profile was taken to be the resonant frequency for the unperturbed ${}^7\text{Li}$ D_1 transition ($\sim 4.46 \times 10^5$ GHz). Once this was performed, the transmitted power was calculated according to

$$P(\nu) = P_0(\nu)e^{-\delta(\nu)}. \quad (5.5)$$

The frequency-dependent amplitude $P_0(\nu)$ was determined by making fits to the linear portions of the observed data (e.g. the region from $\sim 15 - 20$ GHz in Fig. 4.1).

5.2 Comparison of the Model with Data

The computer model mimics only the broadest trends of the observed data, but as can be seen from Fig. 4.1 the two only have qualitative agreement. The encouraging features of the model are (1) it changes from positive to negative at essentially the same locations as the data and (2) it is of the same order of magnitude as the data. The shortfall is its narrower and more intricate features. The most prominent deviation occurs near ~ 5 GHz where the model predicts a double-hump and the data shows a smooth, deeper feature.

5.3 Possible Improvements on Model and Data

Improving the data acquisition could be a first step towards a more agreeable union between the model and data. First, the data can be taken at higher

laser power to strengthen the signal to noise. Additionally the beam can be expanded so that the intensity is not so high that it may potentially affect the population distribution. Another step towards improvement could be to take more data in a more systematic way. For example, it would have been preferable to take all data with the same laser intensity. It also would have been preferable to assign some measure of error to the data.

Many questions and improvements regarding the model can be addressed as well. For example, it was unclear if the laser linewidth should be incorporated into the model. It is possible that broader features in the model could smear out the finer details, hence giving better predictions. Another possibility arises from not accounting for the large hyperfine splitting in the ground state. A model including hyperfine structure was made, but it was known to have errors. Its predictions did not significantly alter the shape of the Faraday rotation from the model presented. However, since it was known to be in error it is not certain whether or not an error-free hyperfine model would do a better job. Finally, once a model whose predictions seem to work has been found, a best fit could be performed to match the free parameters to their optimum values.

Chapter 6

Conclusion and Outlook

The Faraday rotation signal has been observed and a model has been constructed in attempt to explain the features. As predicted the polarization rotation observed is a rapidly varying function of laser frequency in the region near the transitions. While the data and model presented in this thesis have opened the door to Faraday rotation laser spectroscopy, many possible improvements remain undone and many questions unanswered. The magnitude and sign of the model's predictions were consistent with the data, but the model's features were much more intricate than the features in the data. The source of the discrepancy is unknown, but many possibilities can be probed which might lead toward better predictions.

Acknowledgements

This work would not have been possible without the following people. Most importantly, I offer my sincerest gratitude to Dr. Alex Cronin for the guidance, support, and opportunities he has given me. Working in his lab has cemented my desire to become a researcher. I offer my thanks to Dr. Bill Bickel for his laboratory advice, his stockpile of hardware, and his friendship. I would also like to acknowledge Vincent Lonij, Ben McMorran and Dr. John Perrault for their occasional tidbits of lab-savvy. I thank Tori Carr and Yancey Sechrest for their moral support and friendship.

Bibliography

- [1] Alcock, C.B., V.P. Itkin and M.K. Horrigan. *Vapor Pressure Equations for the Metallic Elements: 298-2500 K*. Canadian Metallurgical Quarterly, 23, 309-313 (1984).
- [2] Bransden, B.H. and C.J. Joachain. *Physics of atoms and molecules*. Pearson Education Limited, Essex, England (2003).
- [3] Budker, Dmitry, Derek F. Kimball, David P. DeMille. *Atomic Physics*. Oxford University Press, USA (2004).
- [4] Carr, Adra. *Hyperfine Studies of Lithium Vapor using Saturated Absorption Spectroscopy*. BS Honors Thesis, University of Arizona, Department of Physics (2007).
- [5] Charnock, Forrest T., R. Lopusnik, T.J. Silva. *Pump-probe Faraday rotation magnetometer using two diode lasers*. Review of Scientific Instruments, 76(5) (2005).
- [6] Cronin, Alex. Private communication.
- [7] Demtroder, Wolfgang. *Laser Spectroscopy, 2nd. ed.* Springer-Verlag, Heidelberg, Germany (1981).
- [8] Hecht, Eugene. *Optics, 4th. ed.* Addison-Wesley, Reading, MA, (2001).
- [9] Hffner, J., C. Fricke-Begemann. *Accurate lidar temperatures with narrowband filters*. Opt. Lett. 30, 890-892 (2005).
- [10] Khazanov, E.A. *Characteristic features of the operation of different designs of the Faraday isolator for a high average laser-radiation power*. Quantum Electronics, 30, 147 (2000).

- [11] Metcalf, Harold J., Peter van der Straten. *Laser Cooling and Trapping*. Springer-Verlag, New York (1999).
- [12] Michael Faraday. *Experimental Researches in Electricity*, paragraphs 2146-2242 [in Vol. III of the reprint edition]. Dover, New York, (1965).
- [13] Sechrest, Yancey H. *Laser Spectroscopy of Lithium Vapor: Hole-Burning and the Hanley Effect*. BS Honors Thesis, University of Arizona, Department of Physics (2007).
- [14] Van Baak, D.A. *Faraday Rotation as a Probe of Atomic Dispersion*. Am. J. Phys. 64(6) (1996).